NATIONAL ADVISORY COMMITTEE FOR AERONAUTICS

TECHNICAL NOTE 3099

IMPINGEMENT OF WATER DROPLETS ON AN ELLIPSOID

WITH FINENESS RATIO 5 IN AXISYMMETRIC FLOW

By Robert G. Dorsch, Rinaldo J. Brun, and John L. Gregg

Lewis Flight Propulsion Laboratory
Cleveland, Ohio

NACA

NATIONAL ADVISORY COMMITTEE FOR AERONAUTICS

TECHNICAL NOTE 3099

IMPINGEMENT OF WATER DROPLETS ON AN ELLIPSOID WITH FINENESS

RATIO 5 IN AXISYMMETRIC FLOW

By Robert G. Dorsch, Rinaldo J. Brun, and John L. Gregg

SUMMARY

The presence of radomes and instruments that are sensitive to water films or ice formations in the nose section of all-weather aircraft and missiles necessitates a knowledge of the droplet impingement characteristics of bodies of revolution. Because it is possible to approximate many of these bodies with an ellipsoid of revolution, droplet trajectories about an ellipsoid of revolution with a fineness ratio of 5 were computed for incompressible axisymmetric air flow. From the computed droplet trajectories, the following impingement characteristics of the ellipsoid surface were obtained and are presented in terms of dimensionless parameters: (1) total rate of water impingement, (2) extent of droplet impingement zone, (3) distribution of impinging water, and (4) local rate of water impingement.

INTRODUCTION

All-weather aircraft and missiles frequently have instruments located in the nose section of the fuselage that are sensitive to impinging atmospheric water droplets and ice accretion. For example, it has been found that the operation of an aircraft radar system located in a nose or wing radome is affected by a layer of ice or water distributed over the radome surface. Therefore, it is necessary to evaluate, for given flight conditions, the expected distribution of various sizes of impinging water droplets over the nose section of the aircraft or missile. In addition, problems such as those encountered in the performance of external armament during flight in icing conditions require the evaluation of droplet impingement on bodies of revolution in order to determine where ice will form.

Although a large variety of body shapes are used for radomes, rocket pods, and bombs, the impingement calculations may be made for a body selected to approximate a large group of these practical shapes. A prolate ellipsoid of revolution is a good approximation for many of these bodies, and it has the additional advantage of a flow field that is known exactly for incompressible, nonviscous flow.

The trajectories of atmospheric water droplets about a prolate ellipsoid of revolution with a fineness ratio of 5 moving at subsonic velocities were calculated with the aid of a differential analyzer at the NACA Lewis laboratory. From the computed trajectories, the rate, distribution, and surface extent of impinging water were obtained and are summarized in terms of dimensionless parameters in this report.

SYMBOLS

The following symbols are used in this report:

A   semimajor axis

a   droplet radius, ft

B   semiminor axis

C_D drag coefficient for droplets, dimensionless

d   droplet diameter, microns

d_{med} volume-median droplet diameter, microns

E_m collection efficiency, dimensionless

K   inertia parameter, $\dfrac{2\rho_w a^2 U}{9\mu L}$, dimensionless

K_{med} inertia parameter based on volume-median droplet diameter, dimensionless

L   major axis of ellipse, ft

Re   local Reynolds number with respect to droplet, $2a\rho_a \bar{v}/\mu$, dimensionless

Re_0 free-stream Reynolds number with respect to droplet, $2a\rho_a U/\mu$, dimensionless

$Re_{0,med}$ free-stream Reynolds number based on volume-median droplet diameter, dimensionless

r,z   cylindrical coordinates, ratio to major axis, dimensionless

r_0 starting ordinate at $z = -\infty$ of droplet trajectory, ratio to major axis, dimensionless

$r_{0,tan}$ starting ordinate at $z = -\infty$ of droplet trajectory tangent to ellipsoid surface, ratio to major axis, dimensionless

S   distance along surface of ellipsoid from forward stagnation point to point of droplet impingement, ratio to major axis, dimensionless

S_m limit of impingement zone, ratio to major axis, dimensionless

t   time, sec

U   free-stream velocity, ft/sec; or flight speed, mph, when indicated

u   local air velocity, ratio to free-stream velocity

v   local droplet velocity, ratio to free-stream velocity

$\bar{v}$ magnitude of local vector difference between velocity of droplet and velocity of air, ft/sec

W   rate of impingement of water, lb/hr

W_m total rate of impingement of water on surface of ellipsoid, lb/hr

W_β local rate of impingement of water, lb/(hr)(sq ft)

w   liquid-water content in cloud, g/cu m

α 1/4 focal distance of ellipsoid

β local impingement efficiency, dimensionless

ϵ eccentricity of ellipse defined by a meridian section of ellipsoid of revolution

λ, μ prolate-elliptic coordinates

μ viscosity of air, slugs/(ft)(sec)

ρ_a density of air, slugs/cu ft

ρ_w density of water, slugs/cu ft

τ time scale, tU/L, dimensionless

Subscripts:

r   radial component

z   axial component

ANALYSIS

The flow field around an ellipsoid of revolution in a stream moving in the direction of its major axis is axisymmetric. Therefore, the droplet impingement on the elliptical sections of all meridian planes is the same. Thus, the droplet impingement distribution on an ellipsoid of revolution can be obtained from trajectories in the z,r plane (fig. 1). The coordinates z and r are dimensionless and expressed as ratio of actual distance to major axis length L. The dimensionless equations of motion of the droplet trajectories are of the same form as those derived in reference 1 and can be written

$$\frac{dv_z}{d\tau} = \frac{C_D Re}{24} \frac{1}{K} (u_z - v_z) \tag{1a}$$

$$\frac{dv_r}{d\tau} = \frac{C_D Re}{24} \frac{1}{K} (u_r - v_r) \tag{1b}$$

where

$$K \equiv \frac{2}{9} \frac{\rho_w a^2 U}{\mu L} \tag{2}$$

and $\tau = tU/L$, and all velocities are in the form of ratio of local velocity to free-stream velocity U.

The Reynolds number Re can be obtained conveniently in terms of the free-stream Reynolds number

$$Re_0 = 2a\rho_a U/\mu \tag{3}$$

from the relation

$$\left(\frac{Re}{Re_0}\right)^2 = (u_z - v_z)^2 + (u_r - v_r)^2 \tag{4}$$

The coefficient of drag C_D is a function of Reynolds number. The values of C_D corresponding to various values of Reynolds number are obtained from experimental drag data (ref. 2).

The air velocity components for incompressible nonviscous flow about a prolate ellipsoid of revolution are obtained from the exact solution of Laplace's equation in prolate-elliptic coordinates (fig. 2)

given by Lamb (ref. 3). The details for obtaining the velocity components in the z,r plane from Lamb's potential function in prolate-elliptic coordinates are given in appendix A. The z and r components of the air velocity field can be expressed in the form

$$u_z = - C \left[\frac{1}{\epsilon} \ln \left(\frac{\sqrt{M} + \sqrt{N} + \epsilon}{\sqrt{M} + \sqrt{N} - \epsilon} \right) - \frac{1}{2} \left(\frac{1}{\sqrt{N}} + \frac{1}{\sqrt{M}} \right) \right] + 1 \tag{5}$$

and

$$u_r = - \frac{\epsilon}{2} Cr \left(\frac{1}{\sqrt{M}} - \frac{1}{\sqrt{N}} \right) \frac{1}{z^2 + r^2 + \sqrt{M} \sqrt{N} - \frac{\epsilon^2}{4}} \tag{6}$$

where

$$\sqrt{M} \equiv \sqrt{\left(z + \frac{\epsilon}{2} \right)^2 + r^2}$$

$$\sqrt{N} \equiv \sqrt{\left(z - \frac{\epsilon}{2} \right)^2 + r^2}$$

$$C \equiv \frac{- 1/2}{\frac{1}{2\epsilon} \ln \left(\frac{1+\epsilon}{1-\epsilon} \right) - \frac{1}{1-\epsilon^2}}$$

The constant ϵ is the eccentricity of the ellipse defined by the meridian section of the ellipsoid of revolution. For an ellipse with fineness ratio of 5, $\epsilon = \sqrt{0.96}$. Equations (5) and (6) were solved for several hundred points in the flow field with the use of electronic calculating machines employing punched cards. The values of the air velocity components u_z and u_r as functions of r and z are given in figure 3. Figure 3(a) gives u_z as a function of z for constant values of r, while figure 3(b) gives u_r as a function of r for constant z.

Assumptions that are necessary to the solution of the problem are:

(1) At a large distance ahead of the ellipsoid (free-stream conditions), the droplets do not move with respect to the air.

(2) No gravitational force acts on the droplets.

(3) The droplets are always spherical and do not change in size.

The first two assumptions are valid for droplets smaller than drizzle or rain drops. The assumptions are usually also valid for falling rain drops, because the airplane velocity is usually much greater than the drop velocity caused by gravitational force. Preliminary calculations have shown that the third assumption is valid for the order of accuracy usually required in the design of equipment for the protection of aircraft.

METHOD OF SOLUTION

The differential equations of motion (1) are difficult to solve, because the values of the velocity components and the term containing the coefficient of drag depend on the position of the drop at each instant and, therefore, are not known until the trajectory is traced. The values of these quantities must be fed into the equation as the trajectory of a droplet is developed. This was accomplished by using a mechanical differential analyzer constructed at the NACA Lewis laboratory for this purpose (ref. 1). The answers were obtained in the form of plots of droplet trajectories with respect to the ellipsoid. A typical group of droplet trajectories is shown in figure 4. From the droplet-trajectory plots were obtained the impingement characteristics of interest discussed in subsequent sections.

The equations of motion (1) were solved for various values of the parameter $1/K$ between 0.1 and 90. For each value of the parameter $1/K$, a series of trajectories was computed for each of several values of free-stream Reynolds number Re_0: 0, 128, 512, 1024, 4096, and 8192. In order that these dimensionless parameters have more physical significance in the following discussions, some typical combinations of K and Re_0 are presented in table I in terms of the length and the velocity of the ellipsoid, the droplet size, and the flight pressure altitude and temperature.

Before the integration of the equations of motion to obtain the trajectories could be performed with the differential analyzer, the initial velocity of the droplets had to be determined at the point selected as the starting position. In addition, since the starting position must be selected at a finite distance ahead of the ellipsoid, it was necessary to make a correction to this starting ordinate in order to obtain the corresponding starting ordinate r_0 at $z = -\infty$. Preliminary tests showed that, from $z = -\infty$ to $z = -2$, the trajectories and streamlines were essentially coincident. Furthermore, between $z = -2$ and $z = -1$, the magnitude of the change in the air velocity

components with change in r was negligibly small (fig. 3) compared
with unity on the air velocity scale used in solving the equations.
Consequently, the changes in the droplet velocity and the ordinate r
along a given trajectory between z = -2 and z = -1 were essentially
independent of the starting r value or of the value of Re_0. There-
fore, a trajectory was run between z = -2 and z = -1 for each value
of 1/K in order to obtain the correct starting conditions at z = -1.
By this method it was possible to solve the trajectories starting at
z = -1 so that, within the accuracy of the machine, this would be
equivalent to starting the trajectory at an infinite distance ahead of
the ellipsoid.

In order to minimize errors due to changes in the length of the
paper used on the air velocity input drums caused by humidity and tem-
perature variations, the component velocities of the flow field shown
in figure 3 were plotted on 20- by 30-inch sheets of glass tracing
cloth. A fine grid was laid out on the tracing cloth with a plotting
machine constructed for this purpose. The droplet trajectories (fig. 4)
were plotted by the differential analyzer on sheets of acetate in order
to minimize scale changes and damage due to handling. The r-ordinate
of the trajectory plots was scaled to 4 times the z-ordinate in an
effort to improve the accuracy of determining the point of droplet im-
pingement on the ellipsoid surface. With this distorted scale, the
trajectories were plotted with respect to an ellipsoid section with a
major axis of 30 inches and a minor axis of 24 inches. The accuracy
with which the various droplet impingement characteristics could be
obtained is discussed in the following section.

RESULTS AND DISCUSSION

A series of droplet trajectories about the ellipsoid of revolution
with a fineness ratio of 5 at zero angle of attack was computed for the
various combinations of the dimensionless parameters K and Re_0.
These data are summarized in figure 5, where the starting ordinate r_0
of each trajectory is given as a function of the point of impingement
on the surface S. (S is the distance measured along the surface from
the forward stagnation point to the point of impingement; the relation
between S and z and r is given in appendix B.) The dashed lines
in figure 5 are the loci of the termini of the constant K curves.
These loci were found to be the same, within the order of accuracy of
the computations, for all values of Re_0, as can be seen by comparing
figures 5(a) to (f). The dot-dashed curves among the constant K curves
for $Re_0 = 4096$ and $Re_0 = 8192$ (figs. 5(e) and (f)) were obtained by
interpolation. From the data presented in this figure, the rate, the
area, and the distribution of water-droplet impingement on the surface
of the ellipsoid can be determined for given values of Re_0 and K.

Total Rate of Impingement of Water

In flight through clouds composed of droplets of uniform size, the total amount of water in droplet form impinging on the ellipsoid is determined by the amount of water contained in the volume within the surface formed by the tangent trajectories (fig. 1). Therefore, the total rate of impingement of water (lb/hr) can be determined from the relation

$$W_m = 0.33\pi r_{0,tan}^2 wL^2 U \tag{7}$$

where 0.33 is a conversion factor, the flight speed U is in miles per hour, the liquid-water content w is in grams per cubic meter, and L is in feet. When constants are combined,

$$W_m = 1.04 r_{0,tan}^2 wL^2 U \tag{8}$$

In this equation, $r_{0,tan}^2$ is a measure of the efficiency of catch, because it is proportional to the collection efficiency $(E_m = 100 r_{0,tan}^2)$, defined as the ratio of the actual amount of water intercepted by the ellipsoid to the total amount of water in droplet form contained in the volume swept out by the ellipsoid.

The value of $r_{0,tan}$ for a given combination of Re_0 and K can be obtained from figure 5 by determining the value of r_0 which corresponds to the maximum S for the constant K curve of interest. The values of $r_{0,tan}$ fall on the dashed termini curves of figure 5. In order to facilitate interpolation and extrapolation, the data are replotted in the form of $r_{0,tan}^2$ as a function of K for constant Re_0 in figure 6. Examination of figure 6 shows that $r_{0,tan}^2$ increases with increasing K but decreases with increasing Re_0.

The accuracy of the determination of $r_{0,tan}$ is very much dependent on the shape of the tangent trajectory in the vicinity of the surface of the ellipsoid. For example, for the combination of $1/K = 1$ and $Re_0 = 4096$ shown in figure 4, the shape of the tangent trajectory and its neighboring trajectories is such that a small increase of the order of 0.0007 in r_0 above the true value of $r_{0,tan}$ will result in a trajectory that definitely misses the ellipsoid. A similar slight decrease in the value of r_0 will result in a trajectory that unmistakably impinges on the surface. The tangent trajectory is, therefore, relatively easy

to determine for this case; and $r_{0,tan}$ can, therefore, be determined to an accuracy of the order of ±0.0003. However, for a combination of $1/K$ and Re_0 that results in small values of $r_{0,tan}$, such as shown in figure 4 for $1/K = 30$ and $Re_0 = 512$, the crowding together of the trajectories near the ellipsoid and the tendency of the trajectories to have the same shape as the ellipsoid surface result in a possible question as to the true value of $r_{0,tan}$. Trajectories with r_0 as much as 30 percent smaller than the true value of $r_{0,tan}$ may appear to be tangent. Therefore, in order to avoid selecting a trajectory that is not the tangent when determining $r_{0,tan}$, the value of r_0 was increased by small increments until a trajectory definitely missed the ellipsoid. Thus, an upper limit to the region of possible tangency was established and used as a guide when selecting the tangent trajectory. With this method for determining the tangent trajectory, the accuracy of $r_{0,tan}$ in this Re_0 and K region is within ±0.0007 for values of $r_{0,tan} \geq 0.01$. For reported values of $r_{0,tan} < 0.01$, the accuracy in determining the tangent trajectory is somewhat indefinite, but appears to be within ±0.001.

The effect of body size on the value of $r_{0,tan}^2$ for selected cloud droplet size and flight conditions is illustrated in figure 7. The calculated values given in figure 7 for ellipsoids with a fineness ratio of 5 and major axis lengths between 3 and 300 feet are for flight at 50, 100, 300, or 500 miles per hour through uniform clouds composed of droplets of 10, 20, or 50 microns in diameter at pressure altitudes of 5000, 15,000, or 25,000 feet and temperatures (most probable icing temperature given in ref. 4) of 20°, 1°, and -25° F, respectively. For example, consider a 40-foot-long ellipsoid with a fineness ratio of 5 traveling at 500 miles per hour with zero angle of attack at a pressure altitude of 15,000 feet through a uniform cloud composed of droplets of 20 microns in diameter. From figure 7(b), $r_{0,tan}^2$ is 0.000114. If the liquid-water content of the cloud is assumed to be 0.1 gram per cubic meter, then (from eq. (8)) the total rate of impingement of water W_m is 9.5 pounds per hour.

Extent of Droplet Impingement Zone

The extent of the droplet impingement zone on the surface of the ellipsoid is obtained from the tangent trajectories. The point of tangency determines the rearward limit of the impingement zone. The limit of impingement S_m for a particular Re_0 and K condition can be determined from the maximum S value of the constant K curve of

interest in figure 5. Again, to facilitate interpolation, the data are
replotted in the form of S_m as a function of K for constant Re_0
values in figure 8. The data of this figure indicate that S_m in-
creases with increasing K but decreases with increasing Re_0.

Because of the difficulty of determining the exact point of tan-
gency on the surface of the ellipsoid of each tangent trajectory, the
accuracy of determining S_m is of the order of ±0.005. The accuracy
of determining the value of S for the intermediate points of impinge-
ment given in figure 5 was much higher, because the points at which the
intermediate trajectories terminated on the ellipsoid surface were much
better defined.

The effect of body size on the value of S_m for selected cloud
droplet and flight conditions is illustrated in figure 9. For example,
consider a 20-foot-long ellipsoid with a fineness ratio of 5 traveling
300 miles per hour at zero angle of attack at a 5000-foot pressure
altitude through a uniform cloud composed of 50-micron droplets. From
figure 9(a), S_m is 0.109; that is, the impingement zone extends 2.18
feet rearward (measured along the surface) from the forward stagnation
point.

Distribution of Impinging Water Along Ellipsoid Surface

The amount of water impinging on the ellipsoid surface within any
ring of width $S_2 - S_1$ can be determined if the starting ordinates r_0
are known for the droplets that impinge at S_1 and S_2. These data
can be obtained from figure 5.

The amount of water (lb/hr) impinging within the ring of width
$S_2 - S_1$ is given by the relation

$$W = 1.04(r_{0,2}^2 - r_{0,1}^2)wL^2U \tag{9}$$

Local Rate of Impingement of Water

The local rate of impingement of water in droplet form
(lb/(hr)(sq ft)) on the surface of the ellipsoid can be determined from
the expression

$$W_\beta = 0.33Uw \frac{r_0}{r} \frac{dr_0}{dS} = 0.33Uw\beta \tag{10}$$

where β is the local impingement efficiency. The values of β as a function of S for combinations of Re_0 and K are presented in figure 10. These curves were obtained by multiplying the slope of the curves in figure 5 by the corresponding ratio r_0/r at each point. The dot-dashed curves included for $Re_0 = 4096$ and $Re_0 = 8192$ were obtained from the corresponding interpolated curves of figure 5. Because the slopes of the r_0 against S curves (fig. 5) in the region between $S = 0$ and $S = 0.01$ are difficult to determine, the exact values of β between $S = 0$ and $S = 0.01$ are not known. The values of β presented in this region between $S = 0$ and $S = 0.01$ are estimated to be accurate within ± 0.05.

IMPINGEMENT IN CLOUDS OF NONUNIFORM DROPLET SIZE

The data presented in figures 5 to 10 would apply directly only to flights in clouds composed of droplets that are all uniform in size. The droplets in a cloud, however, may have a range of sizes. Theoretical calculations (ref. 5) and experience in the NACA Lewis icing research tunnel on bodies of revolution have shown that the amount of ice collected when a distribution of droplet sizes is present in the tunnel is considerably greater than that which would be obtained if only droplets of the volume-median size were present. Therefore, if the cloud droplet-size distribution is known or can be estimated, then the data must be accordingly modified (or weighted) before the rate, the extent, and the distribution of droplet impingement on the ellipsoid are calculated.

For a nonuniform cloud, the total rate of impingement of water on the ellipsoid can be determined from equation (8) by using the weighted value of $r_{0,tan}^2$ that corresponds to the droplet-size distribution present in the cloud. The weighted value of $r_{0,tan}^2$ can be obtained by plotting $r_{0,tan}^2$ for each droplet size (based on values of K and Re_0 corresponding to each droplet diam.) as a function of the cumulative volume (in percent) of water corresponding to each droplet size and integrating the resultant curve. For example, consider the cloud droplet-size distribution shown in figure 11. Suppose that the volume-median droplet size is 20 microns, the velocity is 200 miles per hour, the ellipsoid length is 10 feet, the pressure altitude is 5000 feet, and the temperature is 20° F. For these conditions, the value of $Re_{0,med}$ is 117.6 and of K_{med} is 0.03898. The values of Re_0 and K corresponding to other droplet sizes in the distribution are obtained by multiplying $Re_{0,med}$ by d/d_{med} and K_{med} by $(d/d_{med})^2$ and are used

to obtain $r_{0,tan}^2$ (fig. 6) for each droplet size. The values of $r_{0,tan}^2$ for this example are plotted as a function of cumulative volume (in percent) in figure 12. Integration of this curve gives a weighted value of $r_{0,tan}^2$ equal to 0.000425; whereas, the value based on the volume-median droplet size is 0.00031 (fig. 6).

The local rate of impingement of water at any point for a distribution of droplet sizes can be obtained in the same manner. The extent of the droplet impingement zone should be determined from the values of K and Re_0 calculated for the largest droplets present in sufficient number to represent a significant portion of the total water present in the cloud.

CONCLUDING REMARKS

The scale factors used in the differential analyzer to solve the equations for the range of conditions presented in figures 5 to 10 and the near-parallelism of the trajectories to the surface at large values of $1/K$ made it impossible to obtain sufficient accuracy to present detailed data, such as the rate of local impingement of water, at points along the surface of the ellipsoid, for values of $1/K > 90$ for $Re_0 = 0$ and $1/K > 30$ for $Re_0 \geq 128$. From table I it can be seen that, for bodies as large as the fuselage of cargo or passenger airplanes, these conditions are not uncommon. Examination of figures 5 and 10 shows, however, that the extent (usually $S_m < 0.03$) and rate of local impingement are small in this Re_0 and K region. Therefore, in this region a knowledge of the extent of the impingement zone and the total rate of impingement of water as calculated from the data of figures 8 and 6, respectively, is sufficient for most applications.

Because the droplet trajectories about the ellipsoid were calculated for incompressible fluid flow, a question as to their applicability at the higher subsonic velocities may arise. In reference 6 it was shown that the effect of compressibility up to the flight critical Mach number on the trajectories about a cylinder was negligible. In view of the results obtained for the cylinder and of the high flight critical Mach number (greater than 0.9) for the ellipsoid, the ellipsoid impingement results should be applicable for most engineering uses throughout the subsonic region.

The data of this report apply directly only to ellipsoids of revolution with a fineness ratio of 5. Therefore, consideration must be given to the degree of geometric and aerodynamic similarity before

applying the data to bodies of revolution with other shapes. In some cases, where the body is of different shape, it may be possible to match its nose section physically with the nose section of an ellipsoid (fineness ratio, 5) of selected length. If, in such a case, the contribution of the afterbody to the air-flow field in the vicinity of the nose of the body is small (as it often is), then the impingement data for the matching portion of the surface of the ellipsoid can be used for determining the impingement characteristics of the nose region of the body. In other cases, where the body shape differs from that of an ellipsoid but the fineness ratio is the same, the air-flow field may be similar enough that an estimate of the total catch can be obtained from the ellipsoid data. In this case, no details of the surface distribution of impinging water could be obtained. .

Lewis Flight Propulsion Laboratory
    National Advisory Committee for Aeronautics
        Cleveland, Ohio, November 20, 1953

APPENDIX A

CALCULATION OF VELOCITY FIELD ABOUT AN ELLIPSOID OF REVOLUTION

The incompressible nonviscous velocity field for axisymmetric flow about an ellipsoid of revolution can be obtained as follows:

Consider a prolate-elliptic coordinate system in the z,r plane (fig. 1) defined by

$$
\left.\begin{aligned}
z &= \frac{2\alpha}{L} \cosh \zeta \, \cos \eta \\[3mm]
r &= \frac{2\alpha}{L} \sinh \zeta \, \sin \eta
\end{aligned}\right\} \tag{A1}
$$

where

$$0 \leqq \zeta \leqq \infty \quad \text{and} \quad 0 \leqq \eta < 2\pi$$

The coordinates z and r are dimensionless and are expressed as a ratio to the major axis of the ellipsoid of revolution of interest. Examination of equation (A1) shows that ζ = constant and η = constant represent confocal ellipses and hyperbolas, respectively, with a dimensionless semifocal distance of $2\alpha/L$.

Let

$$\lambda = \cosh \zeta$$

and

$$\mu = \cos \eta$$

Then

$$
\left.\begin{aligned}
z &= \frac{2\alpha}{L} \lambda\mu \\[4mm]
r &= \frac{2\alpha}{L} \sqrt{\lambda^2 - 1} \sqrt{1 - \mu^2}
\end{aligned}\right\} \tag{A2}
$$

and

where

$$1 \leqq \lambda \leqq \infty \quad \text{and} \quad -1 \leqq \mu \leqq +1$$

and λ = constant and μ = constant also represent confocal ellipses and hyperbolas, respectively (fig. 2). The major axis of each ellipse is along the z-axis.

The velocity potential expressed in λ,μ coordinates can be obtained from zonal surface harmonics (refs. 3, 7, and 8) and expressed in the following dimensionless form:

$$\Phi = \frac{\Phi'}{UL} = C\mu \left(\frac{1}{2} \lambda \ln \frac{\lambda+1}{\lambda-1} - 1 \right) - \frac{2\alpha}{L} \lambda\mu \tag{A3}$$

where Φ' has the usual dimensions of velocity potential.

For an ellipsoid defined by the surface λ_0 = constant in a fluid moving with a free-stream velocity of U in the direction of the z-axis of the ellipsoid, the constant C is given by

$$C = \frac{\dfrac{2\alpha}{L}}{\dfrac{\lambda_0}{\lambda_0^2-1} - \dfrac{1}{2} \ln \dfrac{\lambda_0+1}{\lambda_0-1}} \tag{A4}$$

The coordinates λ and μ can be expressed in terms of z,r coordinates as follows:

$$\lambda = \frac{1}{\epsilon} \left[\sqrt{\left(z + \frac{\epsilon}{2}\right)^2 + r^2} + \sqrt{\left(z - \frac{\epsilon}{2}\right)^2 + r^2} \right] \tag{A5}$$

and

$$\mu = \frac{1}{\epsilon} \left[\sqrt{\left(z + \frac{\epsilon}{2}\right)^2 + r^2} - \sqrt{\left(z - \frac{\epsilon}{2}\right)^2 + r^2} \right] \tag{A6}$$

where $\epsilon = \frac{2\alpha}{L/2} = \frac{4\alpha}{L}$ is the eccentricity of the ellipse defined by λ_0 = constant. If the surface coordinates of the ellipse of eccentricity ϵ are substituted in (A5), it is found that

$$\lambda_0 = \frac{1}{\epsilon}$$

Then equation (A3) can be expressed in the form

$$\Phi = C\mu \left(\frac{1}{2} \lambda \ln \frac{\lambda+1}{\lambda-1} - 1 \right) - \frac{\epsilon}{2} \lambda\mu$$

where

$$C \equiv \frac{-1/2}{\frac{1}{2\epsilon} \ln \left(\frac{1+\epsilon}{1-\epsilon} \right) - \frac{1}{1-\epsilon^2}} \tag{A7}$$

In addition, equations (A2) take the form

$$z = \frac{\epsilon}{2} \lambda\mu$$

and

$$r = \frac{\epsilon}{2} \sqrt{\lambda^2 - 1} \sqrt{1 - \mu^2}$$

The λ and μ velocity components are obtained from the relations

$$u_\lambda = -\frac{\partial \Phi}{\partial S_\lambda} = \frac{-1}{\frac{\epsilon}{2} \sqrt{\frac{\lambda^2-\mu^2}{\lambda^2-1}}} \frac{\partial \Phi}{\partial \lambda} = -\frac{2}{\epsilon} \sqrt{\frac{\lambda^2-1}{\lambda^2-\mu^2}} \left[C\mu \left(\frac{1}{2} \ln \frac{\lambda+1}{\lambda-1} - \frac{\lambda}{\lambda^2-1} \right) - \frac{\epsilon}{2} \mu \right]$$

$$\tag{A8}$$

and

$$u_\mu = -\frac{\partial \Phi}{\partial S_\mu} = \frac{-1}{\frac{\epsilon}{2} \sqrt{\frac{\lambda^2-\mu^2}{1-\mu^2}}} \frac{\partial \Phi}{\partial \mu} = -\frac{2}{\epsilon} \sqrt{\frac{1-\mu^2}{\lambda^2-\mu^2}} \left[C \left(\frac{1}{2} \lambda \ln \frac{\lambda+1}{\lambda-1} - 1 \right) - \frac{\epsilon}{2} \lambda \right]$$

$$\tag{A9}$$

The z and r velocity components in the z,r coordinate system are obtained from equations (A8) and (A9) as follows:

$$u_z = u_\lambda \frac{\partial z}{\partial \lambda} \frac{d\lambda}{dS_\lambda} + u_\mu \frac{\partial z}{\partial \mu} \frac{d\mu}{dS_\mu} = u_\lambda \; \mu \sqrt{\frac{\lambda^2-1}{\lambda^2-\mu^2}} + u_\mu \; \lambda \sqrt{\frac{1-\mu^2}{\lambda^2-\mu^2}}$$

$$= -\frac{C}{\epsilon} \left(\ln \frac{\lambda+1}{\lambda-1} - \frac{2\lambda}{\lambda^2-\mu^2} \right) + 1 \tag{A10}$$

and

$$u_r = u_\lambda \frac{\partial r}{\partial \lambda} \frac{d\lambda}{dS_\lambda} + u_\mu \frac{\partial r}{\partial \mu} \frac{d\mu}{dS_\mu} = u_\lambda \; \lambda \sqrt{\frac{1-\mu^2}{\lambda^2-\mu^2}} - u_\mu \; \mu \sqrt{\frac{\lambda^2-1}{\lambda^2-\mu^2}} = \left(\frac{2}{\epsilon}\right)^2 \frac{Cr\mu}{\lambda^2-\mu^2} \left(\frac{1}{\lambda^2-1}\right)$$

$$\tag{A11}$$

The velocity components u_z and u_r can be written as a function of z and r by substituting equations (A5) and (A6) into equations (A10) and (A11):

$$u_z = -C \left[\frac{1}{\epsilon} \ln \left(\frac{\sqrt{M} + \sqrt{N} + \epsilon}{\sqrt{M} + \sqrt{N} - \epsilon} \right) - \frac{1}{2} \left(\frac{1}{\sqrt{N}} + \frac{1}{\sqrt{M}} \right) \right] + 1 \tag{5}$$

and

$$u_r = -\frac{\epsilon}{2} Cr \left(\frac{1}{\sqrt{M}} - \frac{1}{\sqrt{N}} \right) \frac{1}{z^2 + r^2 + \sqrt{M} \sqrt{N} - \frac{\epsilon^2}{4}} \tag{6}$$

where

$$\sqrt{M} \equiv \sqrt{\left(z + \frac{\epsilon}{2}\right)^2 + r^2}$$

$$\sqrt{N} \equiv \sqrt{\left(z - \frac{\epsilon}{2}\right)^2 + r^2}$$

and C is given in equation (A7).

The solution of equations (5) and (6) at several hundred points in the flow field for an ellipsoid of revolution with a fineness ratio of 5 ($\epsilon = \sqrt{0.96}$) was accomplished with the use of electronic calculating machines employing punched cards. The values of u_z and u_r as functions of r and z are given in figure 3. Figure 3(a) gives u_z as a function of z for constant values of r, and figure 3(b) gives u_r as a function of r for constant z.

APPENDIX B

RELATION BETWEEN DISTANCE ALONG SURFACE OF ELLIPSE AND z AND r

The length of arc of an ellipse cannot be reduced to an elementary function of z and r, but rather belongs to the class of functions known as elliptic integrals. The length of arc S as a function of z and r is obtained (by the method of ref. 9) as follows:

The equation for an ellipse in the z,r plane can be written parametrically in terms of θ as follows:

$$\left. \begin{array}{l} z = A \sin \theta \\[2mm] r = B \cos \theta \end{array} \right\} \tag{B1}$$

where A and B are, respectively, the semimajor and semiminor axes of the ellipse (fig. 1).

Then

$$dS^2 = dz^2 + dr^2 = \left[A^2 \cos^2\theta + B^2 \sin^2\theta \right] d\theta^2 = \left[A^2 - (A^2 - B^2) \sin^2\theta \right] d\theta^2$$

and

$$S_\theta = A \int_0^\theta \sqrt{1 - \epsilon^2 \sin^2\theta} \; d\theta \tag{B2}$$

where $\epsilon = \dfrac{\sqrt{A^2 - B^2}}{A}$ denotes the eccentricity.

This function is of the form

$$E(k,\theta) = \int_0^\theta \sqrt{1 - k^2 \sin^2\theta} \; d\theta \tag{B3}$$

where

$$0 < k < 1$$

which is known as the Elliptic Integral of the Second Kind in Legendre's form. Tabulated values of this function are available (ref. 10).

For the purposes of this report, the distance along the surface measured from the nose of the body ($z = -0.5$ and $r = 0$) is desired, or,

$$S = A \left(\int_0^{\pi/2} \sqrt{1 - k^2 \sin^2\theta} \, d\theta - \int_0^\theta \sqrt{1 - k^2 \sin^2\theta} \, d\theta \right) . \qquad (B4)$$

where

$$A = 0.5$$

and

$$k^2 = \epsilon^2 = 0.96$$

The relation between S and z computed from equation (B4) is shown in figure 13. The relation between S and r is given by the $1/K = 0$ curve of figure 5, inasmuch as $r = r_0$ for infinitely large values of K.

REFERENCES

1. Brun, Rinaldo J., and Mergler, Harry W.: Impingement of Water Droplets on a Cylinder in an Incompressible Flow Field and Evaluation of Rotating Multicylinder Method for Measurement of Droplet-Size Distribution, Volume-Median Droplet Size, and Liquid-Water Content in Clouds. NACA TN 2904, 1953.

2. Wien, W., and Harms, F., eds.: Handbuch der Experimentalphysik. Teil 4, Bd. 4, Akademische Verdagsgesellschaft M.B.H. (Leipsig), 1932.

3. Lamb, Horace: Hydrodynamics. First Am. ed., Dover Pub., 1945.

4. Brun, Rinaldo J., Gallagher, Helen M., and Vogt, Dorothea E.: Impingement of Water Droplets on NACA 65_1-208 and 65_1-212 Airfoils at 4° Angle of Attack. NACA TN 2952, 1953.

5. Lenherr, F. E., and Young, R. W.: Computation of Water Catch on Axial Symmetric Aircraft Radomes. TDM-77, Northrop Aircraft, Inc., Dec. 17, 1952. (Prog. Rep. III, AF 33(038)-1817.)

6. Brun, Rinaldo J., Serafini, John S., and Gallagher, Helen M.: Impingement of Cloud Droplets on Aerodynamic Bodies as Affected by Compressibility of Air Flow Around the Body. NACA TN 2903, 1953.

7. Kaplan, Carl: Potential Flow About Elongated Bodies of Revolution.
      NACA Rep. 516, 1935.

8. Durand, William Frederick: Aerodynamic Theory. Vol. I-VI. Durand
      Reprinting Comm., 1943.

9. Osgood, William F.: Introduction to the Calculus. The MacMillan
      Co. (New York), 1922.

10. Peirce, B. O.: A Short Table of Integrals. Third ed., Ginn and
      Co., 1929.

TABLE I. - RELATION OF DIMENSIONLESS PARAMETERS TO BODY SIZE AND ATMOSPHERIC AND FLIGHT CONDITIONS

Pressure altitude, ft

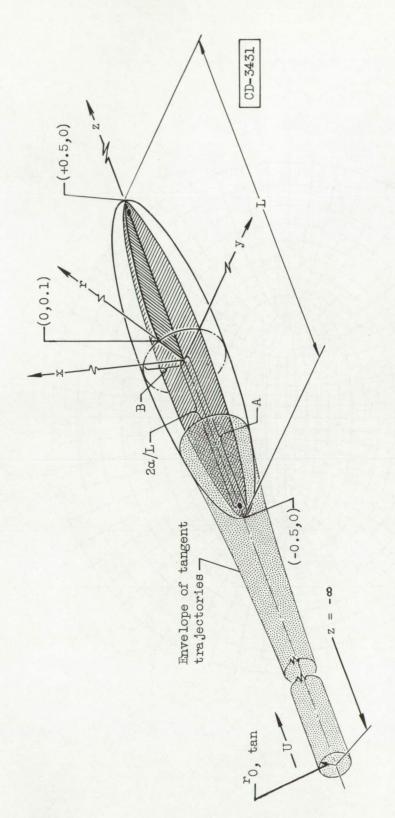| Atmospheric condition	Ellipsoid velocity, U, mph	Droplet diameter, d, microns	Major axis, L, ft	5000					15,000					25,000				
				20					1					-25				
				Re_0	K	1/K	$r^2_{0,tan}$ (fig. 6)	S_m (fig. 8)	Re_0	K	1/K	$r^2_{0,tan}$ (fig. 6)	S_m (fig. 8)	Re_0	K	1/K	$r^2_{0,tan}$ (fig. 6)	S_m (fig. 8)
Cloud droplets	50	10	3	14.7	0.008123	123.1	0.00006	0.017	10.72	0.008383	119.3	0.00006	0.018	7.836	0.008793	113.7	0.00006	0.018
			30	14.7	.0008123	1231	0	0	10.72	.0008383	1193	0	0	7.836	.0008793	1137	0	0
			100	14.7	.0002437	4103	0	0	10.72	.0002515	3976	0	0	7.836	.0002638	3791	0	0
		50	3	73.54	0.2031	4.924	0.00224	0.165	53.62	0.2096	4.771	0.00249	0.182	39.17	0.2198	4.550	0.00272	0.199
			30	73.54	.02031	49.24	.00012	.034	53.62	.02096	47.71	.00017	.038	39.17	.02198	45.50	.00021	.042
			100	73.54	.006092	164.1	.00002	.012	53.62	.006289	159.0	.00003	.013	39.17	.006594	151.7	.00003	.013
	100	20	10	58.81	0.01949	51.31	0.00014	0.038	42.89	0.02012	49.70	0.00018	0.039	31.34	0.02110	47.39	0.00021	0.043
			50	58.81	.003898	256.5	.00001	.007	42.89	.004024	248.5	.00002	.008	31.34	.00422	237.0	.00002	.008
			300	58.81	.0006497	1539	0	0	42.89	.0006707	1491	0	0	31.34	.0007033	1422	0	0
	300	20	10	176.4	0.05846	17.11	0.00042	0.060	128.7	0.06037	16.56	0.00049	0.062	94.00	0.06330	15.8	0.00062	0.071
			50	176.4	.01169	85.54	.00002	.019	128.7	.01267	82.85	.00002	.020	94.00	.01266	78.99	.00004	.023
		10	100	88.2	0.001462	684.0	0	0	64.4	0.001509	662.7	0	0	47.01	0.001583	631.7	0.00001	0.001
		20	100	176.4	0.005846	171.1	0.00001	0.009	128.7	0.006037	165.6	0.00001	0.010	94.00	0.006330	158.0	0.00002	0.012
			300	176.4	.001949	513.1	.00001	.001	128.7	.002012	497.0	.00001	.002	94.00	.002110	473.9	.00001	.002
	500	20	10	294.1	0.09745	10.26	0.00073	0.076	214.5	0.1006	9.940	0.00084	0.084	156.7	0.1055	9.479	0.00095	0.090
			50	294.1	.01949	51.31	.00007	.027	214.5	.02012	49.70	.00009	.028	156.7	.02110	47.39	.00008	.030
			100	294.1	.009745	102.6	.00001	.016	214.5	.01006	99.40	.00001	.016	156.7	.01055	94.79	.00001	.017
		50	3	735.4	2.031	0.4924	0.00590	0.351	536.2	2.096	0.4771	0.00637	0.375	391.7	2.198	0.4550	0.00680	0.392
			30	735.4	.2031	4.924	.00100	.096	536.2	.2096	4.771	.00118	.109	391.7	.2198	4.550	.00154	.125
			100	735.4	.06092	16.41	.00024	.043	536.2	.06289	15.90	.00030	.047	391.7	.06594	15.17	.00041	.054
Drizzle	100	400	10	1176	7.796	0.1283	0.00840	0.448	857.7	8.050	0.1242	0.00865	0.458	626.7	8.442	0.1185	0.00886	0.468
	300	400	100	3529	2.339	0.4275	0.00377	0.247	2574	2.415	0.4141	0.00455	0.283	1880	2.532	0.3949	0.00553	0.313
			300	3529	.7797	1.283	.00132	.113	2574	.8050	1.242	.00190	.150	1880	.8440	1.185	.00253	.180
	500	400	300	5682	1.299	0.7698	0.00176	0.136	4289	1.342	0.7452	0.00206	0.155	3134	1.407	0.7107	0.00278	0.202
Rain	300	1000	50	8823	29.24	0.03420	0.00832	0.446	6434	30.18	0.03313	0.00873	0.457	4701	31.66	0.03159	0.00896	0.466
			100	8823	14.62	.06840	.00702	.390	6434	15.09	.06627	.00766	.418	4701	15.83	.06317	.00813	.435
			300	8823	4.873	.20520	.00388	.263	6434	5.030	.1988	.00480	.300	4701	5.277	.1895	.00550	.325

Temperature, °F

Figure 1. - Coordinate system for droplet trajectory calculations about an ellipsoid of revolution of fineness ratio 5.
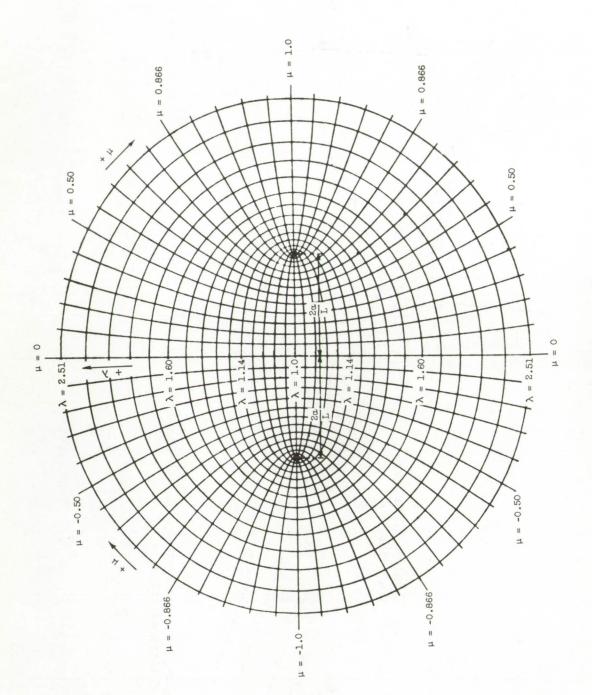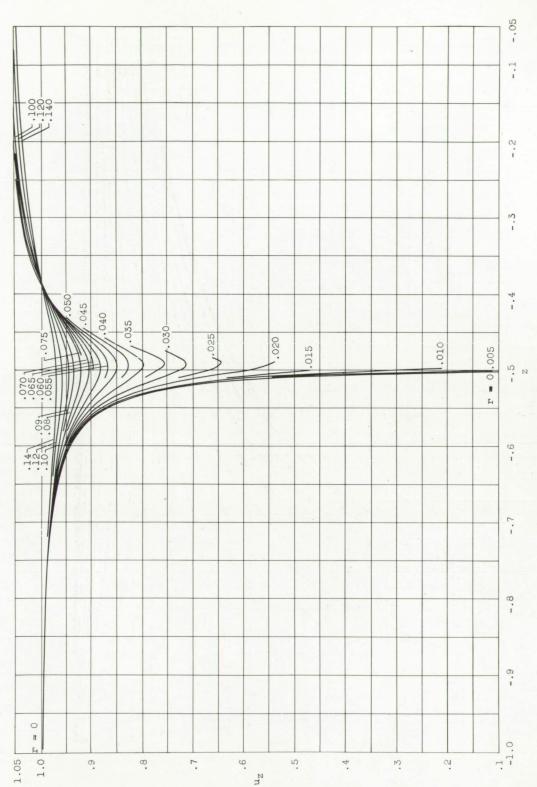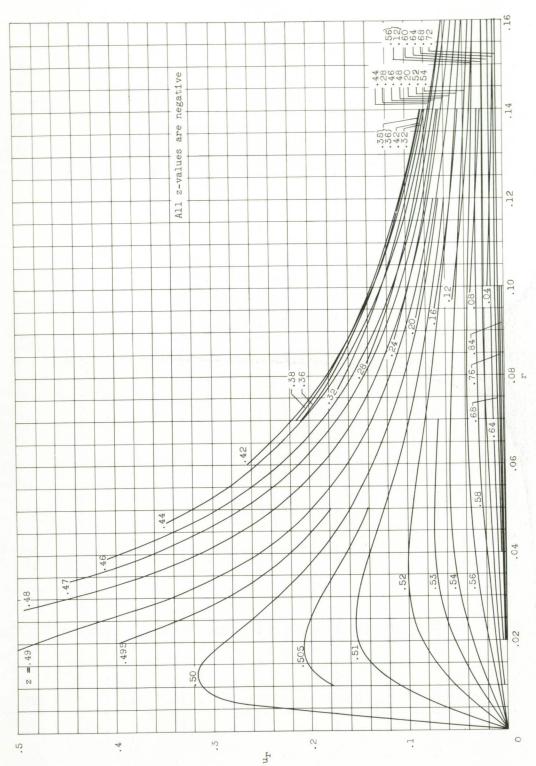
Figure 2. - Prolate-elliptic coordinate system.

(a) z-Component of air velocity as function of z for constant values of r.

Figure 3. - Ellipsoid flow field.

(b) r-Component of air velocity as function of r for constant values of z.

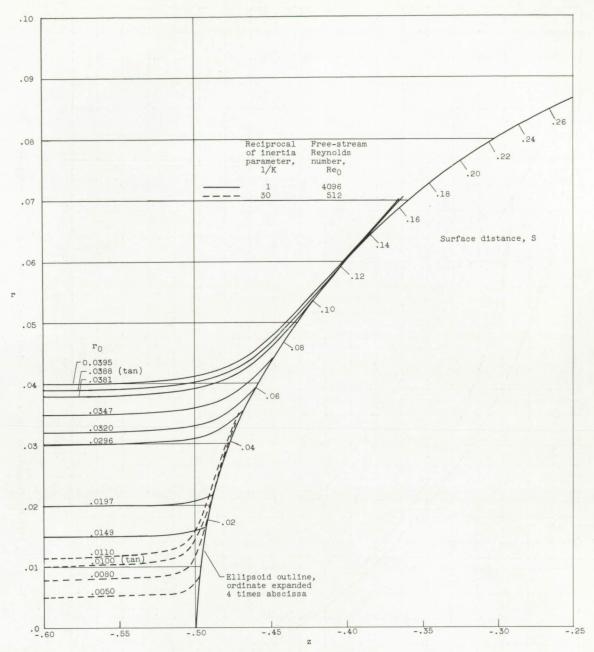Figure 3. - Concluded. Ellipsoid flow field.

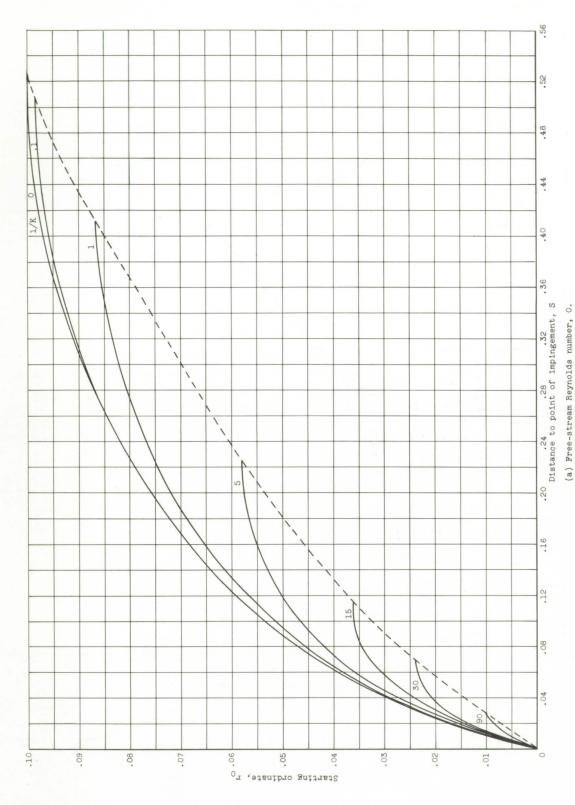Figure 4. - Trajectories of droplets with respect to ellipsoid.

Figure 5. - Starting ordinate as function of distance along surface to point of impingement.
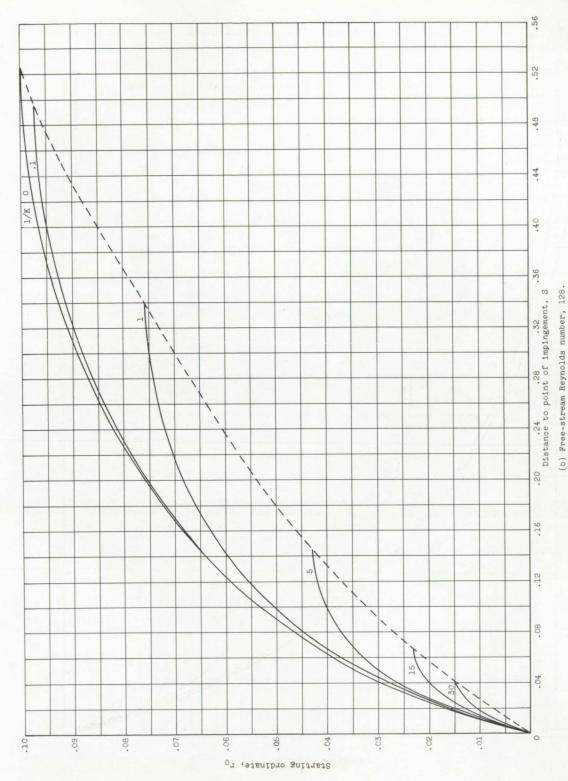
(a) Free-stream Reynolds number, O.

(b) Free-stream Reynolds number, 128.

Figure 5. - Continued. Starting ordinate as function of distance along surface to point of impingement.

(c) Free-stream Reynolds number, 512.

Figure 5. - Continued. Starting ordinate as function of distance along surface to point of impingement.

(d) Free-stream Reynolds number, 1024.

Figure 5. - Continued. Starting ordinate as function of distance along surface to point of impingement.

(e) Free-stream Reynolds number, 4096.

Figure 5. - Continued. Starting ordinate as function of distance along surface to point of impingement.

Figure 5. - Concluded. Starting ordinate as function of distance along surface to point of impingement.
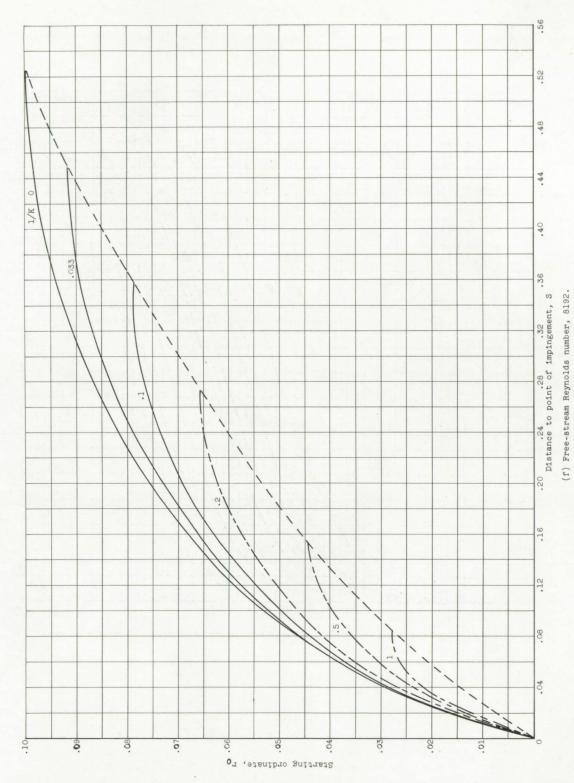
(f) Free-stream Reynolds number, 8192.

Distance to point of impingement, S

Starting ordinate, r_0

1/K
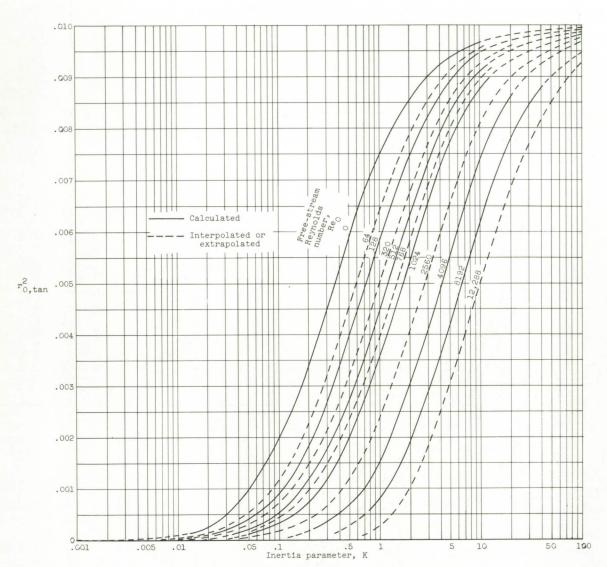
Figure 6. - Square of starting ordinate of tangent trajectory as function of inertia parameter.

(a) Pressure altitude, 5000 feet; temperature, 20° F.
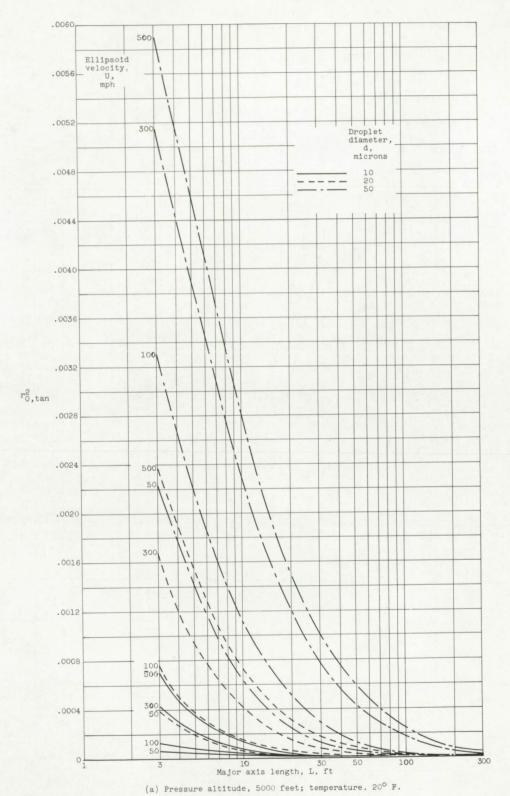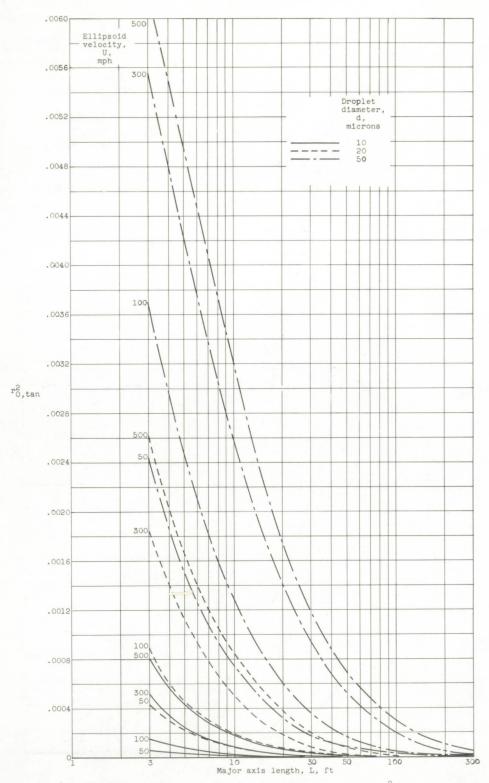
Figure 7. - Square of starting ordinate of tangent trajectory as function of major axis length of ellipsoid.

(b) Pressure altitude, 15,000 feet: temperature, 1° F.

Figure 7. - Continued. Square of starting ordinate of tangent trajectory as function of major axis length of ellipsoid.

(c) Pressure altitude, 25,000 feet; temperature, -25° F.
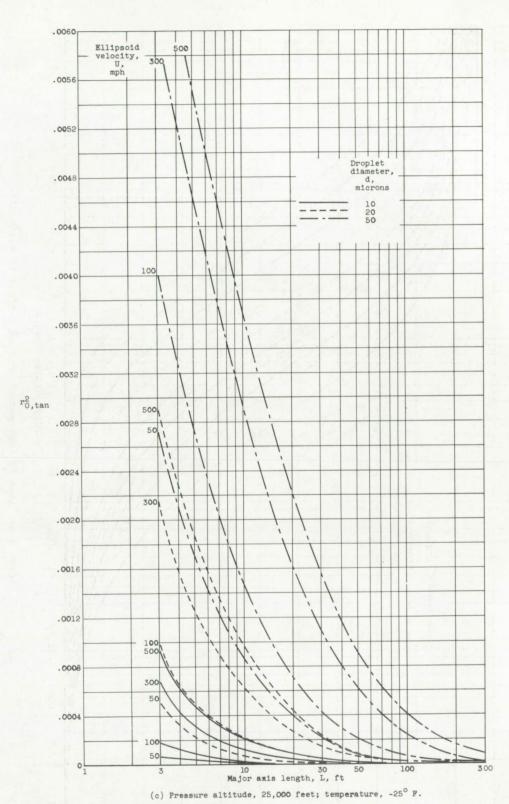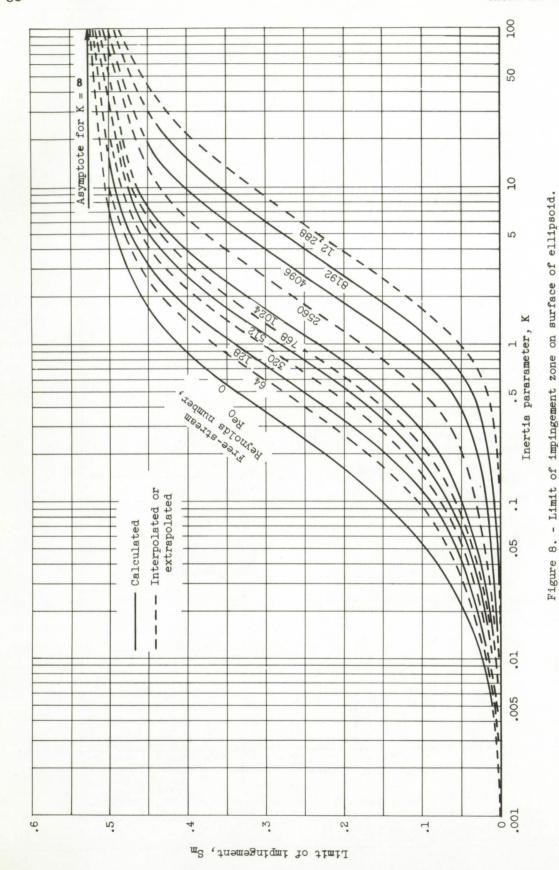
Figure 7. - Concluded. Square of starting ordinate of tangent trajectory as function of major axis length of ellipsoid.

Figure 8. - Limit of impingement zone on surface of ellipsoid.

(a) Pressure altitude, 5000 feet; temperature, 20° F.
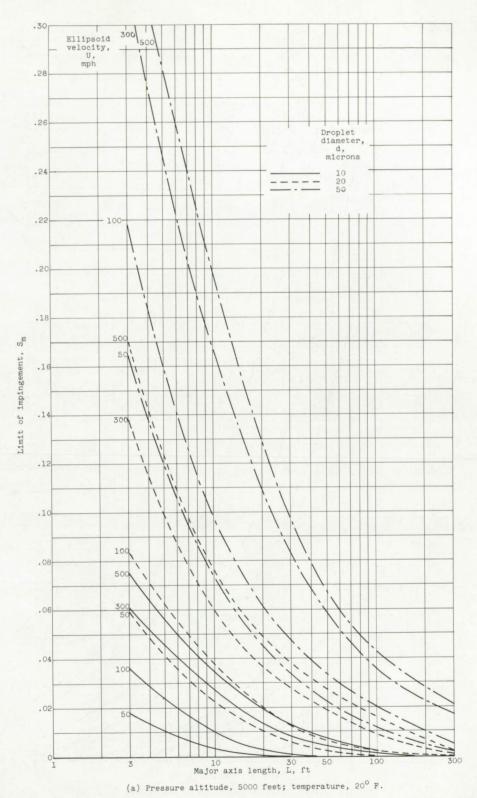
Figure 9. - Maximum extent of impingement zone as function of major axis of ellipsoid.

(b) Pressure altitude 15,000 feet; temperature, 1° F.
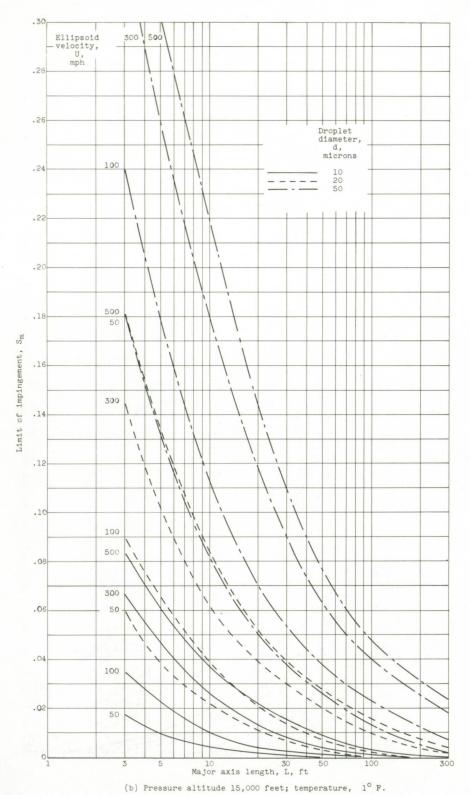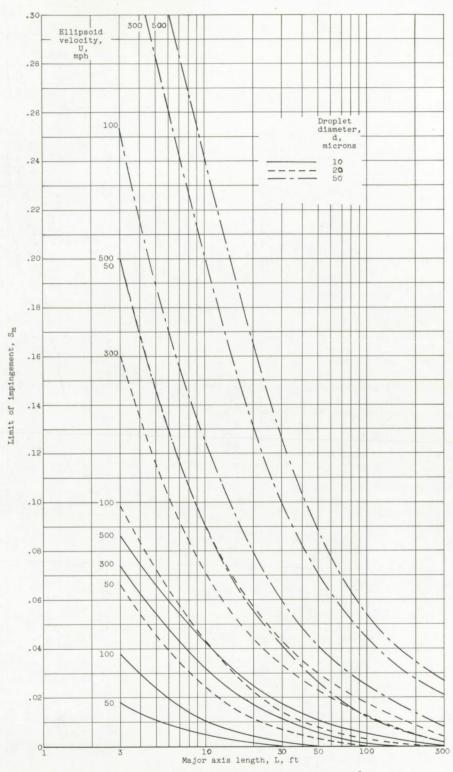
Figure 9. - Continued. Maximum extent of impingement zone as function of major axis
of ellipsoid.

(c) Pressure altitude, 25,000 feet; temperature, -25° F.

Figure 9. - Concluded. Maximum extent of impingement zone as function of major axis of ellipsoid.

Distance along surface to point of impingement, S

(a) Free-stream Reynolds number, O.
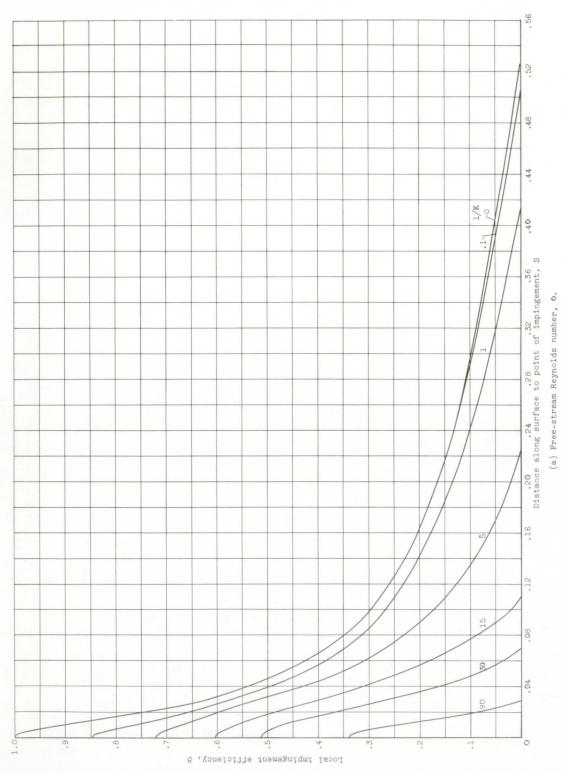
Figure 10. - Local impingement efficiency: $\beta = \dfrac{r_0}{r}\dfrac{dr_0}{dS}$.

Local impingement efficiency, β

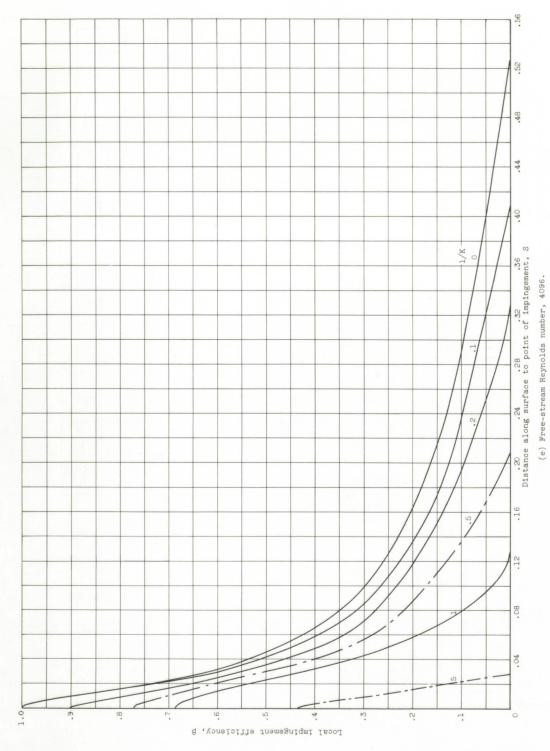Figure 10. - Continued. Local impingement efficiency: $\beta = \dfrac{r_0}{r}\dfrac{dr_0}{dS}$

(b) Free-stream Reynolds number, 128.

Distance along surface to point of impingement, S

Local impingement efficiency, β

(c) Free-stream Reynolds number, 512.

Figure 10. - Continued. Local impingement efficiency: $\beta = \dfrac{r_0}{r}\dfrac{dr_0}{dS}$.

(d) Free-stream Reynolds number, 1024.

Figure 10. – Continued. Local impingement efficiency: $\beta = \dfrac{r_0}{r}\dfrac{dr_0}{dS}$.

(e) Free-stream Reynolds number, 4096.

Figure 10. - Continued. Local impingement efficiency: $\beta = \dfrac{r_0}{r} \dfrac{dr_0}{dS}$.

Figure 10. – Concluded. Local impingement efficiency: $\beta = \dfrac{r_0}{r}\dfrac{dr_0}{dS}$.
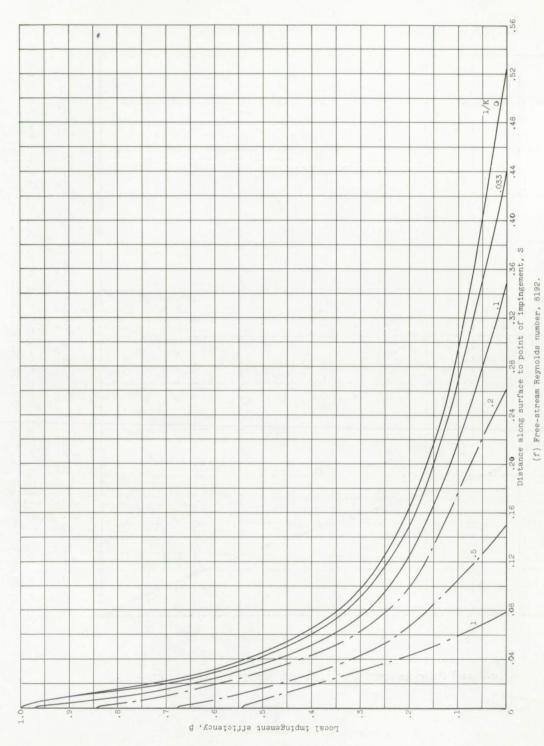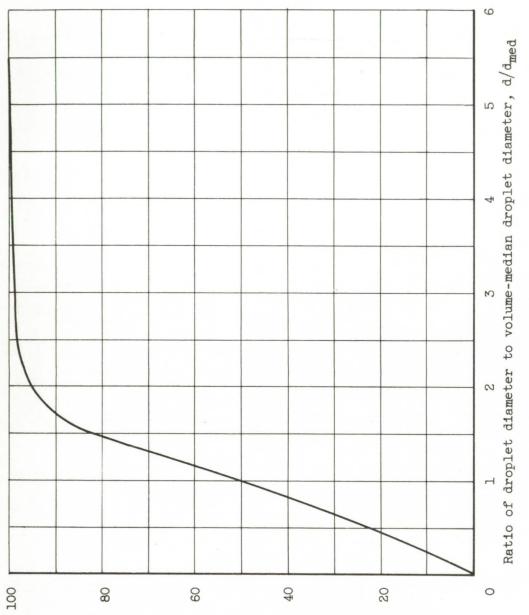
(f) Free-stream Reynolds number, 8192.

Figure 11. - Typical cloud droplet-size distribution in NACA Lewis icing research tunnel. Volume-median droplet diameter, 20 microns.

Ratio of droplet diameter to volume-median droplet diameter, d/d_{med}
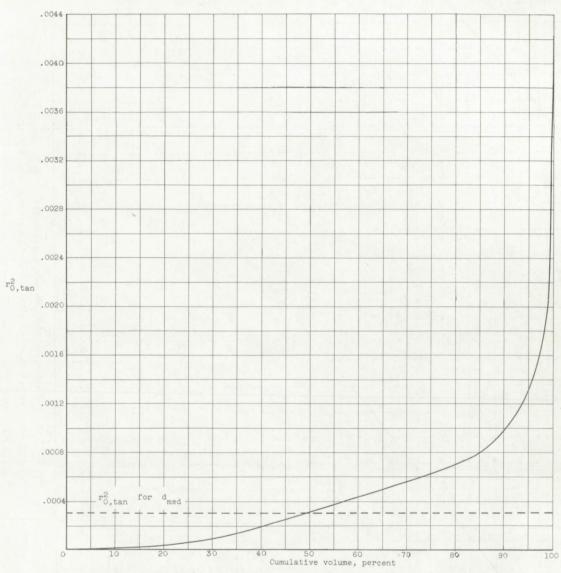
Cumulative volume of total cloud water, percent

Figure 12. - Relation of $r_{0,tan}^2$ to cumulative volume of water corresponding to droplet size from which $r_{0,tan}$ is determined. Area under curve gives $(r_{0,tan}^2)_{weighted} \approx 0.000425$.
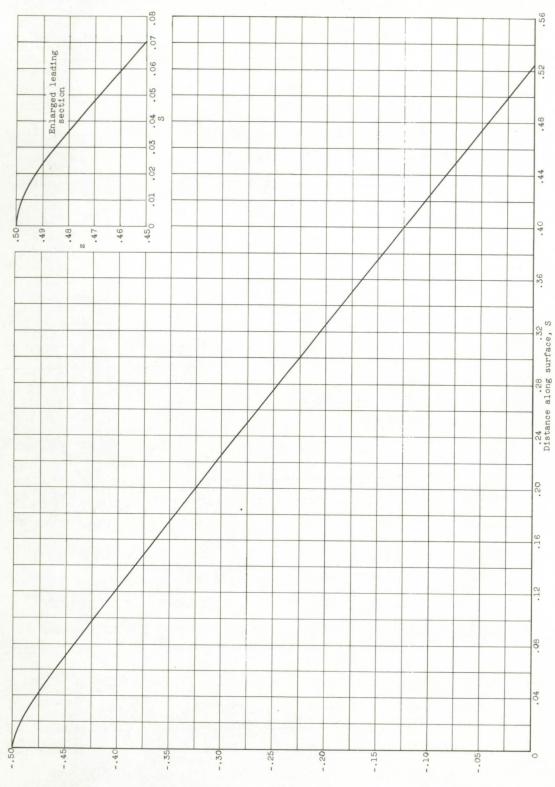
Figure 13. - Relation between distance along ellipsoid surface and z-coordinate.